ELSEVIER

A contour dynamics algorithm for axisymmetric flow

Karim Shariff [a,*], Anthony Leonard [b], Joel H. Ferziger [c]

[a] *NASA Ames Research Center, Moffett Field, CA 94035, United States*
[b] *Graduate Aeronautical Laboratories, California Institute of Technology, Pasadena, CA 91125, United States*
[c] *Flow Physics and Computation, Stanford University, Stanford, CA 94305, United States*

Abstract

The method of contour dynamics, developed for two-dimensional vortex patches by Zabusky et al. [N.J. Zabusky, M.H. Hughes, K.V. Roberts, Contour dynamics for the Euler equations in two-dimensions, J. Comp. Phys. 30 (1979) 96–106] is extended to vortex rings in which the vorticity distribution varies linearly with normal distance from the symmetry axis. The method tracks the motion of the boundaries of the vorticity regions and hence reduces the dimensionality of the problem by one. We discuss the formulation and implementation of the scheme, verify its accuracy and convergence, and present illustrative examples.
© 2007 Elsevier Inc. All rights reserved.

1. Introduction

In two-dimensions, the contour dynamics approach, initiated by Zabusky et al. [34], has made possible the study of the inviscid motion of vortex patches containing piecewise constant vorticity; see Pullin [28] for a review. Since vorticity follows the fluid, such a distribution remains unaltered in time within each region and only the boundaries between regions have to be tracked as they convect with the fluid velocity. The velocity can be expressed as a line integral along the contours, thus reducing the dimensionality of the problem by one. The approach was inspired by the so-called water-bag method in magnetohydrodynamics; for a recent work see [12]. In principle, arbitrary vorticity distributions may be approximated by piecewise constant ones, but to date most of the work has focussed on vortices containing single regions.

Contour dynamics has yielded mathematical insight into the nature of solutions of the Euler equations as well as increased understanding of physical processes in shear layers and two-dimensional turbulence. For instance Dritschel [7,8] elucidated the role of energetics in the merger and fission of vortices and in more

---

* Corresponding author. Tel.: +1 650 604 5361.
  E-mail addresses: kshariff@mail.arc.nasa.gov (K. Shariff), tony@galcit.caltech.edu (A. Leonard).

general topological changes that occur during their long time evolution. Specifically, perturbations of equilibrium solutions tend asymptotically to different equilibrium states which are energetically compatible with the original state. Dritschel [10] also studied nearly inviscid two-dimensional turbulence on a sphere using this approach and his results sharply contrast with behavior observed under the more viscous conditions of spectral simulations. Neu [21], motivated to explain the genesis of streamwise braid vortices in mixing layers, showed that highly flattened uniform vorticity cores ''collapse'' to a circular shape with concentrated vorticity when subjected to a three-dimensional strain which models the influence of spanwise rollers and neighboring streamwise vortices. Lin and Corcos [17], using finite-difference calculations of the two-dimensional Navier–Stokes equations with out of plane strain confirmed the mechanism for an array consisting of counter rotating pairs. Pullin and Jacobs [29] provided further evidence with contour dynamics simulations of vortex arrays employing multiple contours. As a final example, we mention [33] who studied some aspects of entrainment into a turbulent boundary layer by considering the behavior of disturbances on a uniform vorticity layer near a wall.

This work extends the method of contour dynamics to vortex rings in the hope that it may play a similar role in providing insight for axisymmetric flow that contour dynamics has for planar flows. The extension to axisymmetric flow offers the possibility of expanding the repertoire of possible vortex behavior by allowing an important effect lacking in planar flow, namely vortex stretching.

Section 2 gives a derivation of the contour dynamics formulation for the case in which ω_ϕ/σ (the ratio of azimuthal vorticity to cylindrical radius) is constant within each vorticity region. This form of the vorticity has been studied for over a century. Helmholtz [14] already started deriving the speed of translation of thin rings of this class in his 1858 paper and Kelvin put the finishing touches to the derivation in an appendix to the 1867 translation of Helmholtz' paper. In 1894 Hill presented his famous spherical vortex, an exact steadily translating vortex in the thick core limit (see [1, p. 526]). Norbury [22] provided numerical solutions for the family of steadily propagating rings between the thin-core and Hill limits. Some dynamical aspects have also been studied. This includes Dyson's [11] model from 1893 of thin interacting rings (for which core dynamics can be neglected) and the stability analysis of Hill's vortex by Moffatt and Moore [20].

Section 3 discusses the numerical implementation of the algorithm, including treatment of the local contribution to the velocity field resulting from those portions of the contour which neighbor the point at which the velocity is evaluated. Section 4 verifies the accuracy and convergence of the numerical scheme. Finally, §5 presents two examples: the behavior of an axisymmetric annular vortex layer and the head-on collision of two vortex rings. Appendix A provides details on the local contribution to the velocity field and Appendix B works out an expression for the Stokes' streamfunction ψ in terms of a contour integral which might prove useful to those who wish to find steadily translating configurations; it also helps in computing the energy which is proportional to the integral of the product of ψ and the azimuthal vorticity ([1, p. 521]).

The present formulation and implementation was developed in the summer of 1984. Around the same time Pozrikidis independently also developed a contour dynamics formulation for axisymmetric flow and his work was reported in Pozrikidis [27] in which he studied the instability of Hill's vortex in the non-linear regime. We will remark on the significant differences between the two formulations where appropriate. In 1990, Möhring sent us a 1978 diploma thesis by Poppe [26] containing a contour formulation for the streamfunction which the author uses to calculate some generalizations of Norbury's rings [22] containing nested contours. Poppe's contour formulation for the streamfunction appears to be different than the present one which is provided in Appendix B.

2. Axisymmetric contour dynamics formulation

In this section we derive the equations of motion for contours which bound regions in which the vorticity is a linear function of the cylindrical radius, σ. The reason for using this distribution will be given below.

Consider cylindrical polar coordinates (x, σ, ϕ) as shown in Fig. 1; x and σ measure distance along and normal to the axis of symmetry, respectively, and ϕ is the azimuthal angle. Let the vorticity $\boldsymbol{\omega}$ be entirely azimuthal and independent of ϕ:
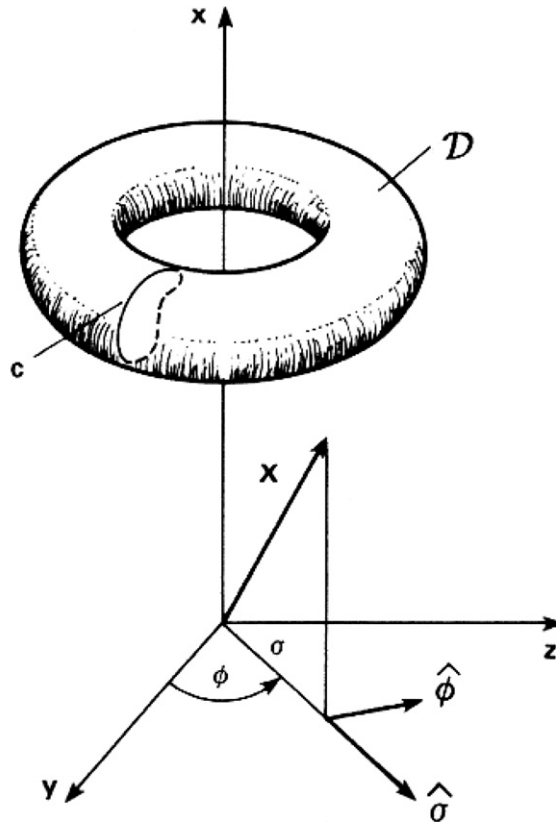
Fig. 1. Cylindrical coordinates.

$$\boldsymbol{\omega} = (0, 0, \omega_\phi(x, \sigma)). \tag{1}$$

The corresponding velocity field is

$$\mathbf{u} = (u_x(x, \sigma), \quad u_\sigma(x, \sigma), 0). \tag{2}$$

Then for inviscid, incompressible, and barotropic flow the vorticity obeys the evolution equation [1, p. 508]:

$$\frac{D(\omega_\phi/\sigma)}{Dt} = 0. \tag{3}$$

The inclusion of the radius σ in (3) is a consequence of the fact that a circular vortex line which moves from a radius σ_1 to a radius σ_2 undergoes a change in vorticity proportional to σ_2/σ_1, i.e., according to the relative change in its circumference. If, in some region $\mathcal{D}$, we initially have

$$\omega_\phi = \mathcal{A}\sigma, \tag{4}$$

where $\mathcal{A}$ is a constant for the region, then this distribution is maintained for all time. To solve (3) it is then necessary to follow only the interfaces between such regions which are advected according to the local fluid velocity. An equation similar to (3) also holds in helical coordinates, the radius σ being replaced by the metric appropriate to that coordinate system; a contour dynamics formulation should also in principle be possible in this case.

We now seek a representation of the velocity field in terms of line integrals along the generators of the bounding surfaces of the vortical regions. Several vortex structures may be present and there may be several nested regions within each structure, but, for brevity of the presentation and notation we will only consider the case of a single vorticity region with zero vorticity outside of it. Multiple and nested regions are treated by superposition. A kinematic relation between the velocity and vorticity is the Poisson equation

$$\nabla^2 \mathbf{u} = -\nabla \times \boldsymbol{\omega}, \tag{5}$$

whose inversion for an unbounded fluid yields the Biot–Savart expression

$$\mathbf{u}(\mathbf{x}) = \frac{1}{4\pi} \int_{\mathcal{D}} \frac{\nabla' \times \boldsymbol{\omega}(\mathbf{x}')}{r} \, \mathrm{d}\mathbf{x}'. \tag{6}$$

Here, $r \equiv |\mathbf{x} - \mathbf{x}'|$ is the distance between the source and field points and ∇' is the del operator with respect to the source point $\mathbf{x}'$. In his numerical study of steadily translating rings, Norbury [22] used a formulation based on the Stokes streamfunction which is more convenient than a velocity formulation for calculating steady shapes. Reduction to contour integrals was not made and this necessitated costly plane quadratures. In Appendix B we obtain a contour reduction for the Stokes streamfunction which might prove useful in studying steady solutions more complicated than Norbury's [22] family, for instance periodic arrays or rings with nested regions.

For future use we note that in cylindrical coordinates

$$r^2 = A - B\cos(\phi - \phi'), \tag{7}$$

where

$$A \equiv (x - x')^2 + \sigma^2 + \sigma'^2, \tag{8}$$
$$B \equiv 2\sigma\sigma'. \tag{9}$$

For an axisymmetric distribution of vorticity $\omega_\phi = \omega_\phi(x,\sigma), \omega_x = \omega_\sigma = 0$, the curl of the vorticity which appears in the integrand of (6) is

$$\nabla \times \omega(\mathbf{x}) = \frac{1}{\sigma} \frac{\partial(\omega_\phi \sigma)}{\partial \sigma} \hat{\mathbf{x}} - \frac{\partial \omega_\phi}{\partial x} \hat{\sigma}. \tag{10}$$

The vorticity suffers jumps at the boundary of the vortical region so the derivatives above must be interpreted in the sense of distributions. In two-dimensional flow with uniform vorticity, $\nabla \times \omega(\mathbf{x})$ is non-zero only where jumps in vorticity occur and so a formulation in terms of contour integrals is almost immediate. In the present situation $\nabla \times \boldsymbol{\omega}(\mathbf{x}) = 2\mathcal{A}\hat{\mathbf{x}}$ (a constant) inside $\mathcal{D}$, a Dirac δ concentrated on the boundary $\partial\mathcal{D}$ due to the vorticity jump, and zero outside $\mathcal{D}$. Hence, it is convenient to decompose the velocity field, as given by (6), into a contribution due to the continuous vorticity distribution and another due to the vorticity jump across the boundary:

$$\mathbf{u} = \mathbf{u}_c + \mathbf{u}_j. \tag{11}$$

2.1. Jump contribution to the velocity field

One way of obtaining $\mathbf{u}_j$ is to evaluate the Biot–Savart integral over a shell of thickness 2ε surrounding $\partial\mathcal{D}$ and then take the limit of zero ε. This is best accomplished by transforming to an orthogonal surface oriented coordinate system (n, s, ϕ) as shown in Fig. 2. To ensure unit metrics let n and s measure arc length along the respective coordinate lines. The metric for the ϕ coordinate lines is the radius σ. If θ is the angle, with respect to the axis of symmetry, of the normal direction, then these coordinates are described by the transformation

$$\begin{pmatrix} \mathrm{d}n \\ \mathrm{d}s \\ \mathrm{d}\phi \end{pmatrix} = \begin{pmatrix} \cos\theta(s,n) & \sin\theta(s,n) & 0 \\ -\sin\theta(s,n) & \cos\theta(s,n) & 0 \\ 0 & 0 & 1 \end{pmatrix} \begin{pmatrix} \mathrm{d}x \\ \mathrm{d}\sigma \\ \mathrm{d}\phi \end{pmatrix}. \tag{12}$$

On the surface of the vortex, $n = 0$, one has $\theta(s,n) = \theta(s)$, the orientation of the outward pointing normal relative to the axis of symmetry. Expressing (10) in this system, we obtain

$$\nabla \times \boldsymbol{\omega}(\mathbf{x}) = \left(\frac{\partial\omega_\phi}{\partial n} \sin\theta(s,n) + \frac{\partial\omega_\phi}{\partial s} \cos\theta(s,n) + \frac{\omega_\phi}{\sigma} \right)\hat{\mathbf{x}} - \left(\frac{\partial\omega_\phi}{\partial n} \cos\theta(s,n) - \frac{\partial\omega_\phi}{\partial s} \sin\theta(s,n) \right)\hat{\sigma}. \tag{13}$$
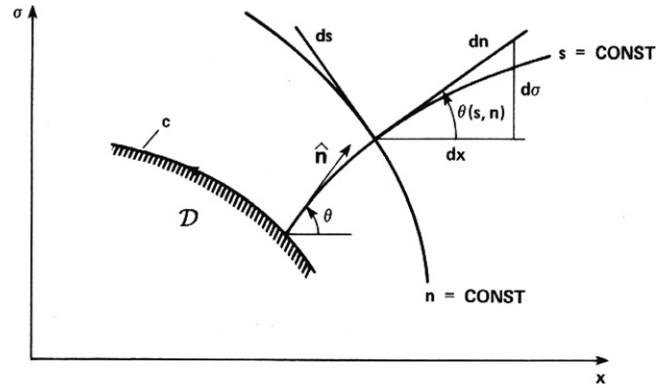
Fig. 2. Surface oriented coordinates (n, s, ϕ) defined in the text.

Upon insertion of this expression into the Biot–Savart Eq. (6), the contributions of the tangential derivatives, being finite, vanish in the limit as ε tends to zero, as does the last term in the first parenthesis. This leaves only normal derivatives of the vorticity; each becomes the jump in vorticity, $-\mathcal{A}\sigma'$, after integration over the direction normal to the surface. Thus we are left with

$$\mathbf{u}_j = \frac{\mathcal{A}}{4\pi} \oint_c \sigma'^2 \mathrm{d}s' \int_0^{2\pi} \frac{-\sin\theta' \hat{\mathbf{x}} + \cos\theta' \hat{\boldsymbol{\sigma}}'}{r} \mathrm{d}\phi', \tag{14}$$

where the contour c is the generator of the surface in the meridional plane. The numerator of the inner integrand is the unit vector tangent to the surface in this plane. The unit vector $\hat{\boldsymbol{\sigma}}'$ in the radial direction depends on the integration variable ϕ' and must be retained inside the integration, in particular

$$\hat{\boldsymbol{\sigma}}' = \cos\phi' \hat{\mathbf{y}} + \sin\phi' \hat{\mathbf{z}}, \tag{15}$$

from Fig. 1. Substituting (15) into (14), choosing to evaluate the velocity on the xy plane ($\phi = 0$), and identifying $\hat{\mathbf{y}}$ with $\hat{\boldsymbol{\sigma}}$ on this plane, gives

$$\mathbf{u}_j = \mathcal{A} \oint_c \mathbf{K}_j(s') \mathrm{d}s', \tag{16}$$

where

$$\mathbf{K}_j(s') = \sigma'[-G(s')\sin\theta' \hat{\mathbf{x}} + H(s')\cos\theta' \hat{\boldsymbol{\sigma}}], \tag{17}$$

$$G(s') \equiv \frac{\sigma'}{4\pi} \int_0^{2\pi} \frac{1}{r} \mathrm{d}\phi', \tag{18}$$

$$H(s') \equiv \frac{\sigma'}{4\pi} \int_0^{2\pi} \frac{\cos\phi'}{r} \mathrm{d}\phi'. \tag{19}$$

The integrals G and H, obtained from Gradshteyn and Ryzhik [13, 2.571.4] and Bierens de Haan [2, Table 68, item 25], respectively, are

$$G(s') = \frac{\sigma'}{\pi\sqrt{A+B}} K(\tilde{r}), \tag{20}$$

$$H(s') = \frac{1}{2\pi\sigma} \left(\frac{A}{\sqrt{A+B}} K(\tilde{r}) - E(\tilde{r})\sqrt{A+B} \right), \tag{21}$$

$$\tilde{r} \equiv \sqrt{\frac{2B}{A+B}}, \tag{22}$$

in which K and E are the complete elliptic integrals of the first and second kind respectively, $\tilde{r}$ is their argument (called the modulus) and A and B are defined in (8) and (9).

2.2. Contribution due to the continuous part of the vorticity

After substituting the fact that $\nabla' \times \boldsymbol{\omega}(\mathbf{x}') = 2\mathcal{A}\hat{\mathbf{x}}$ inside $\mathcal{D}$ into the Biot–Savart expression (6) one obtains the contribution $\mathbf{u}_c$ to the velocity field arising from the continuous part of the vorticity distribution:

$$\mathbf{u}_c = \left(\frac{\mathcal{A}}{2\pi}\int_{\mathcal{D}}\frac{1}{r}\mathrm{d}\mathbf{x}'\right)\hat{\mathbf{x}}. \tag{23}$$

The crucial fact which allows transformation of the volume integral in (23) to a surface integral is the following:

$$\frac{1}{r} = \frac{1}{2}\nabla'^2 r = \frac{1}{2}\nabla'\cdot\nabla' r, \tag{24}$$

which can be checked (use Cartesian coordinates).

Use of (24) together with Gauss' theorem transforms (23) to

$$\mathbf{u}_c = \left(\frac{\mathcal{A}}{4\pi}\int_{\partial\mathcal{D}}\hat{\mathbf{n}}'\cdot\nabla' r\,\mathrm{d}S\right)\hat{\mathbf{x}}. \tag{25}$$

Gauss' theorem is valid provided the integrand $1/r$ is regular. This holds for field points exterior to $\mathcal{D}$ but fails otherwise. However, one can apply the theorem to a region which excludes a spherical region of radius ϵ about the singularity for interior field points and excludes a similar hemispherical region for field points on the surface. It can then be shown that the volume and surface integrals arising from the excluded region vanish in both cases as $\epsilon \to 0$. This renders (25) valid everywhere.

For an axisymmetric surface the integrand in (25) can be simplified as follows. First, write the quantity ∇r in Cartesian coordinates:

$$\nabla' r = -\frac{1}{r}[(x-x')\hat{\mathbf{x}} + (y-y')\hat{\mathbf{y}} + (z-z')\hat{\mathbf{z}}]. \tag{26}$$

Next put $y = \sigma$ and $z = 0$, our previous choice of the azimuthal location of the field point, $y' = \sigma'\cos\phi'$ and $z' = \sigma'\sin\phi'$. From Fig. 2, we observe that the normal vector can be expressed as

$$\hat{\mathbf{n}}' = \cos\theta'\hat{\mathbf{x}} + \sin\theta'\hat{\boldsymbol{\sigma}}' \tag{27}$$

$$= \cos\theta'\hat{\mathbf{x}} + \sin\theta'\cos\phi'\hat{\mathbf{y}} + \sin\theta'\sin\phi'\hat{\mathbf{z}}. \tag{28}$$

Substituting (26) and (28) into (25) and expressing the resulting integral in terms of the quantities, G and H defined previously we obtain

$$\mathbf{u}_c = \mathcal{A}\oint_c \mathbf{K}_c(s')\mathrm{d}s', \tag{29}$$

where

$$\mathbf{K}_c(s') = \{G(s')[(x'-x)\cos\theta' + \sigma'\sin\theta'] - H(s')\sigma\sin\theta'\}\hat{\mathbf{x}}. \tag{30}$$

2.3. Summary of the formulation

Finally, combining the two contributions (16) and (29) to the velocity field and invoking the dynamical fact that the boundary is convected with the fluid, the contour dynamics formulation for axisymmetric flow reads

$$\frac{\mathrm{d}\mathbf{x}(s)}{\mathrm{d}t} = \mathcal{A}\oint_c \mathbf{K}(s')\mathrm{d}s', \tag{31}$$

where

$$\mathbf{K}(s') = [(x'-x)G(s')\cos\theta' - \sigma H(s')\sin\theta']\hat{\mathbf{x}} + \sigma' H(s')\cos\theta'\hat{\boldsymbol{\sigma}}. \tag{32}$$

The formulation of [27] differs from ours in the following respects. The radial component of the velocity arises from the jump contribution only. For it, Pozrikidis' formulation is identical to ours. The difference lies in the treatment of the axial component of the velocity. Pozrikidis expresses the velocity potential external to the vortex as an integral over the core, of the potential due an elemental vortex filament, which can be written in terms of elliptic integrals of the third kind. To obtain the axial velocity this expression is differentiated with respect to x and Green's theorem in the plane is used to secure a contour integral for the velocity. A branch cut is introduced to make the velocity single valued. The final expression involves the elliptic integral of the third kind which can be written in terms of complete and incomplete elliptic integrals of the first and second kind. The latter can be computed iteratively. The present formulation is in terms of the complete elliptic integrals which are calculated by a log-polynomial approximation.

3. Numerical implementation

Eq. (31) is a non-linear integro-differential equation for motion of the boundaries of the vortex cores. For numerical purposes, the contours are represented by a discrete set of node points which are convected as material particles. The integrals are approximated by connecting the points with straight line segments. In the planar case, the segment integrals are carried out in closed form. However, quadrature is sometimes used to save computing time. This requires that the singularity be removed with integration by parts. In the axisymmetric case, neither of these approaches is possible. Instead, just the contribution to the integrals from segments not adjacent to the field point is evaluated by two-point Gaussian quadrature. The elliptic integrals are calculated using the log-polynomial approximations of [4]; the formula which is accurate to 10^{-8} is being used. The cost of the method scales as $N^2 n_q$ where N and n_q are the number of node points and quadrature points per segment, respectively. This is because for each node point $N n_q$ integrand evaluations are needed.

Due to the logarithmic singularity of the integrand as the modulus $\tilde{r} \to 1$, the contribution from segments neighboring the field point is evaluated by expanding the terms in (32) in a series of powers and logarithms about the singularity along an adjacent segment. This series is then integrated exactly term by term. The expansions obtained using MACSYMA have the form

$$\mathbf{K}(\xi) = \mathbf{P}_1^J(\xi) + \mathbf{P}_2^J(\xi) \log\left(\frac{8\xi}{l}\right), \tag{33}$$

where $\mathbf{P}_i^J$ denotes a polynomial of degree J with vector coefficients, l is the length of the segment and ξ is a parameter along the segment such that $0 \leqslant \xi \leqslant 1$. The coefficients of the polynomials depend upon the segment geometry and are listed in Appendix A.

To assess the number of terms in the expansion necessary for accuracy and to check the analysis we compared the values of the integrand for several J against the kernels obtained using the expressions of Cody to evaluate the elliptic integrals. This comparison is meaningful because Cody's expressions have the proper analytic behavior of the elliptic integrals in the limits $\tilde{r} \to 0$ and $\tilde{r} \to 1$. For example, Fig. 3 shows the approximations for the case of a segment for Hill's vortex spanning an arc between polar angles $\vartheta = 25°$ and $\vartheta = 75°$ measured from the forward stagnation point. This length is much larger than any we used in the simulations yet the representation using five terms is accurate throughout the segment.

Fig. 4 compares the exact and computed axial velocity on the surface of Hill's vortex using only 15 segments of identical length. It serves as a check of the overall formulation and underscores the care with which the logarithmic contribution to the velocity must be treated. The results are excellent, the error at the point of maximum velocity being 4%. The dashed curve shows the result obtained when the contribution of adjacent segments is deleted. One observes that away from the axis the contribution from adjacent segments is substantial.

There is a standard approach for treating singular kernels which arise frequently in potential theory (see for example the book by Jawson and Symm [15]). This technique was adopted by Pozrikidis [27]. Here, one subtracts out just the singular part of the kernel. In our formulation this would be the constant term in $\mathbf{P}_2^J(\xi)$ times the log factor. The integral of this term over the entire contour is then be computed exactly for the segment or circular arc discretization and added back in. The non-singular part of the kernel is integrated using Gaussian quadrature. The present approach also accurately integrates terms like $\xi \log \xi$, $\xi^2 \log \xi$, etc., near the singularity which polynomial based quadrature rules are not designed for. On the other hand, since $\log(\xi)$ is
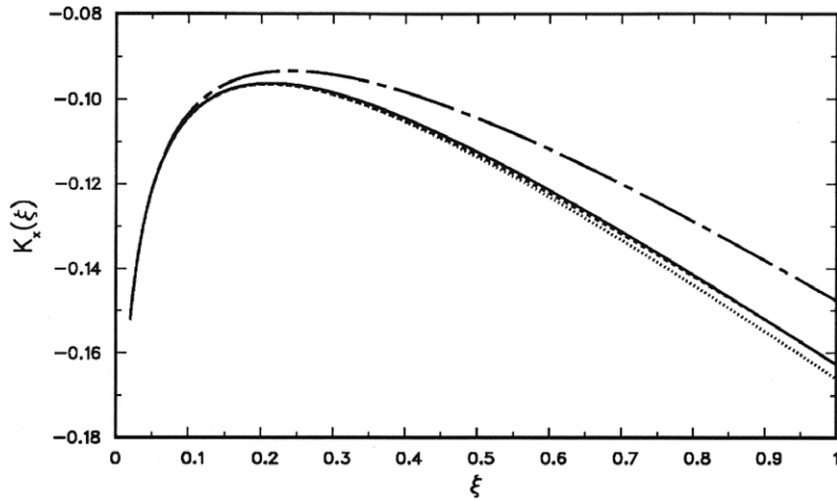
Fig. 3. Integrand for the axial velocity along the chord of an arc between 25° and 75° on a Hill's vortex with unit radius. ——, exact; - - - -, 5 term expansion; ...., 3 terms; – - –, 2 terms.
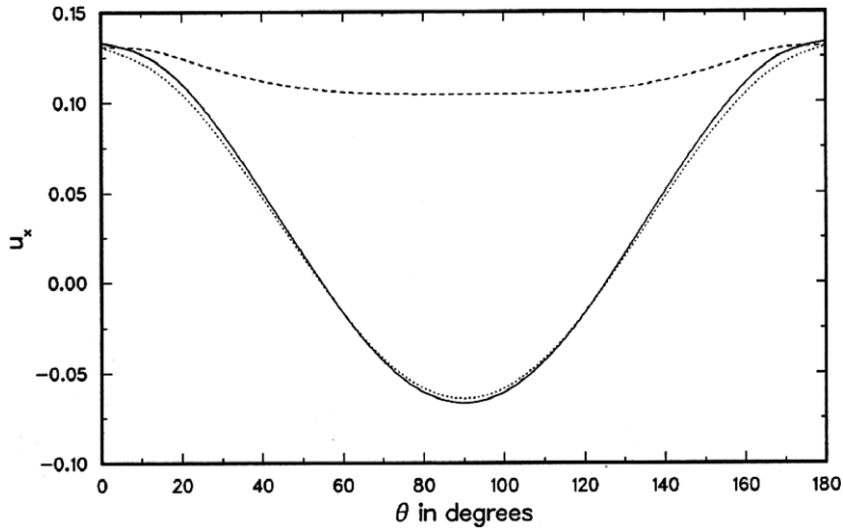

Fig. 4. Axial velocity at node points on a Hill's vortex of unit radius and $\mathcal{A} = 1$. ——, exact; ...., computed with 15 segments; – – –, deleting the contribution from adjacent segments.

weakly varying this might be a non-issue. In Pozrikidis' approach one can in principle increase the number of quadrature points arbitrarily to obtain the desired accuracy. With our approach, apart from the algebra required, the series remains truncated and segments must be kept short to maintain accuracy. The simplest and most direct approach for treating elements (straight or curved) adjacent to a node which has emerged in the boundary element literature is to use a quadrature rule [5] that can exactly integrate:

$$I(\xi) = \int_0^1 [p^J(\xi) + q^J(\xi) \log \xi] \mathrm{d}\xi \tag{34}$$

where $p^J(\xi)$ and $q^J(\xi)$ are polynomials of degree J; Crow provides weights and abscissae for $J \leqslant 6$. For subsequent developments the reader may consult the references in Smith [32].

The present program halves the length of segments which have stretched beyond a specified tolerance (currently $0.016L_0$) and removes nodes when segments become too short ($<0.004L_0$) provided the curvature is sufficiently small. Here, L_0 is the initial mean toroidal radius of the vortex rings. It is also essential that

the length of segments close to the axis of symmetry be kept much less than the distance of the segment from the axis. This is because the expansion of the elliptic integrals on a segment adjacent to a node proceeds in powers and logarithms of the complementary modulus, $r^* = \sqrt{1 - \tilde{r}^2}$ which is small all along the segment provided the length l of the segment is much smaller than the minimum radius $\sigma_{\min}$ of the segment (see the discussion near Eq. (49) in Appendix A). The node insertion routine ensures that $l/\sigma_{\min} < 0.15$ if this condition is more stringent than previous criteria. This criterion is impossible to satisfy for an axis touching segment for which we consider two sub-cases: (i) If the field point is the end point of the segment lying on the axis ($\sigma = 0, x = 0$, say) then the radial velocity is zero by symmetry while for the axial velocity, the integrand tends to zero as the integration point (x', σ') approaches the field point. Thus there is no singularity in this case and quadrature is used. (ii) If the node point is not on the axis then numerical tests indicated that for segments sufficiently close to being axis-normal, the series is still accurate even though the modulus $\tilde{r}$ varies from 0 to 1, its entire range. Before an implementation is undertaken in the future, it would be worthwhile to make a brief study of the accuracy and ease of implementation of all the options available for integration.

Another issue, which we do not address here, is the treatment of non-adjacent segments that are closer to an evaluation point than the length of the segment. This situation arises when filamentary structures are produced or when vortices fission or merge; such events are a generic feature of vorticity dynamics. In the present implementation we stop the calculation before such situations arise. One way to deal with this would be by "contour surgery" (Dritschel [9]) with removes contour portions that are close and anti-parallel. In his work, Pozrikidis [27] also implemented removal of filamentary regions that arise when Hill's spherical vortex is perturbed. In two-dimensions the need to employ contour surgery arises somewhat later in time because the velocity induced by a segment can be computed exactly. In our case a node point that comes close to a segment "sees" only the two quadrature points on the segment which are an inadequate sample of a rapidly varying integrand. The simplest approach to maintain accuracy would be to use adaptive quadrature until it becomes too expensive and then to use contour surgery.

Time integration was performed using the fourth order Runge–Kutta scheme. In initial tests it was found that too large a time step resulted in a shrinking volume of vortical fluid. The time step Δt was chosen to satisfy

$$\Omega \Delta t < \epsilon, \qquad (35)$$

where Ω is half the vorticity at the center of the core and represents the magnitude of the eigenvalues of the ODE system for a particle undergoing solid body rotation at angular velocity Ω. Numerical tests indicated that a constraint in volume change of $\Delta V/V < 0.01\%$ over one eddy turnover period dictated that $\epsilon < 0.05$. The time step restriction from the angular motion can be eliminated by moving each node point according to the contour-normal velocity (since the tangential velocity does not alter the shape of the contour). This is possible in a better than linear representation of the contour where an accurate normal is available at node points.

The amount of insight that one may obtain from a contour dynamics run and confidence in it are increased by extensive diagnostics. To gauge the accuracy of a calculation we monitor the flow invariants: volume, circulation, impulse and, occasionally due to cost, the energy together with its spectrum $E(k)$. The overall motion of the vortices was obtained by calculating the positions of the centroids of the core shape and of the vorticity distribution. Their corresponding time-rates were also monitored. It is not enough to merely visually observe the core shape. This remark also applies to vortex calculations via finite difference or spectral methods. Even very weak strains caused by the presence of another vortex result in the excitation of small but complex deformation modes. Hence the overall features of the core deformation were obtained by fitting an ellipse to the core shape. The dimensions and orientation of the ellipse are related to the eigenvalues and eigenvectors of the matrix of second order moments.

4. Tests of accuracy and convergence

Fig. 5 shows the convergence in the discrete L^2 norm of the axial and radial velocity as a function of the number of segments in the case of Hill's vortex. The slope is close to -2, consistent with the second order accuracy of the segment discretization. There is a slight decrease in the slope as we approach machine round-off (single precision for this test). This represents a static test of the algorithm. A good dynamic test (suggested to us by Prof. Zabusky) is to ensure that for Norbury [22] equilibrium shapes, the core remains
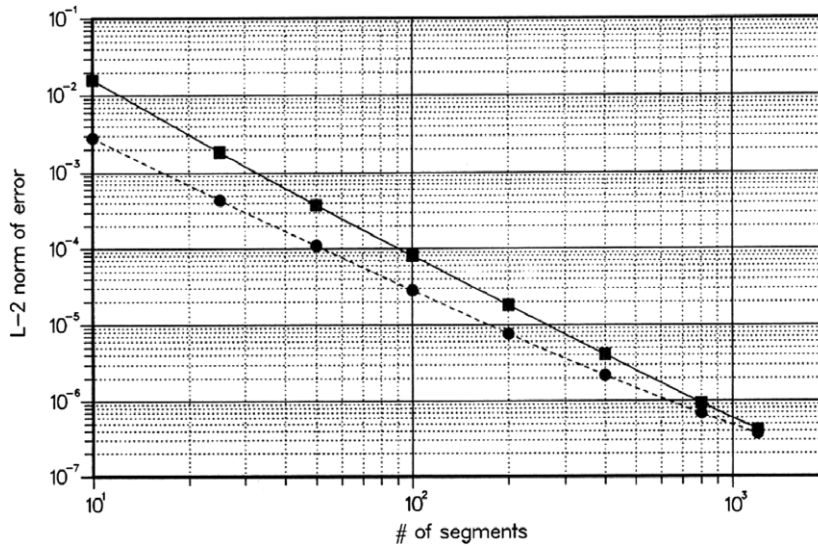
Fig. 5. Error in velocities evaluated at the node points of a Hill's vortex with unit radius and $\mathcal{A} = 1$. ■, ●, for the axial and radial component, respectively.

steady up to the accuracy of the Fourier coefficients in his paper. Adopting the mean toroidal radius L_0 as a reference length, Norbury [22] specifies the boundary by

$$\frac{\varrho(\beta)}{L_0} = \hat{a}_0 + \sum_{j=1}^{J}(\hat{a}_j \cos j\beta + \hat{b}_j \sin j\beta). \tag{36}$$

The initial shapes are symmetric in x, about $x = 0$ say, ϱ is measured from the point $x = 0$, $\sigma = L_0$ and β runs counterclockwise from the point of maximum σ on the line $x = 0$. We studied the excursions of the coefficients from the values supplied by Norbury for the duration of three revolutions of a particle on the boundary for an $\alpha = 0.6$ vortex. Here α is the ratio of area-effective core radius $\left(\sqrt{\text{Area}/\pi}\right)$ to L_0. The observed deviations must have two parts. The first reflects inherent unsteadiness due to errors in the initial shape; a 'cautious' estimate of the error in the initial coefficients is ± 0.0001 according to Norbury. The second is due to inaccuracies in the present method; runs with $200, 400, 800$, and 1200 segments were made to check that it converged to zero. An overall measure of the departure from the initial shape is the quantity

$$\text{rms deviation} = \left(2(\delta\hat{a}_0)^2 + \sum_{j=1}^{J}(\delta\hat{a}_j)^2 + (\delta\hat{b}_j)^2\right)^{1/2}, \tag{37}$$

which is equal, by Parseval's identity, to

$$\left(\frac{1}{\pi L_0^2}\int_0^{2\pi}(\delta\varrho(\beta))^2 d\beta\right)^{1/2}, \tag{38}$$

where δ signifies the difference from the Norbury value and $J = 11$, the number of coefficients furnished by Norbury.

The results are shown in Fig. 6. Normalized time is defined as

$$\hat{t} \equiv \frac{U_0 t}{L_0} \tag{39}$$

where U_0 is the ring translational speed and L_0 is its mean toroidal radius. By 1200 segments the behavior has visually converged and nearly repeats every particle revolution; individual coefficients exhibit the same periodicity. A small but otherwise arbitrary disturbance on a two-dimensional circular vortex with uniform vorticity is also periodic according to Kelvin's analysis because the period of particle revolution is an integer
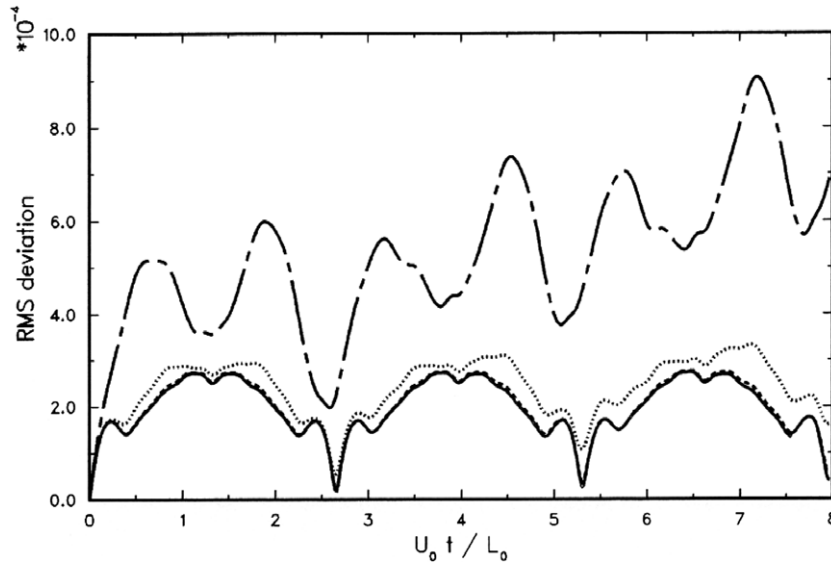
Fig. 6. History of the rms deviation of Fourier coefficients of the core boundary from the initial Norbury [22] shape for different number of segments N_s. – · –, $N_s = 200$; ......, $N_s = 400$; – – –, $N_s = 800$; —, $N_s = 1200$. Note: The ordinate *values* are multiplied by 10^{-4} not the axis title.

multiple of the period required for any Fourier mode to advance one wavelength. A power law fit to the rms deviations at the last instant produced an order of convergence of 2.3, consistent with the segment discretization. The amplitude of the rms deviation for 1200 nodes is less than that obtained by applying Norbury's bound to every coefficient. The maximum variation was observed in $\hat{a}_2$ with an amplitude of 0.00008, close to Norbury's estimate.

5. Examples

As a qualitative illustration of the method, we simulated a Hill's spherical vortex with a region of vortical fluid removed. The removed region has as its initial boundary, one of the interior streamsurfaces of Hill's vortex. The time evolution is shown in Fig. 7 where the shading indicates the vorticity containing region. Time $\hat{t}$ has been normalized using the mean toroidal radius and speed of translation of a Hill's vortex without the hole. A violent evolution occurs during the time that the centroid of the outer boundary has propagated 2.5 radii. Irrotational fluid pushes through the rear, forming a thin cap. The vortex layer at the outer radii thickens in spots as it rolls-up. This illustrates that distinct vortex patches can form from vortex layers by a fast convective action without the intervention of the mechanisms of roll-up into a spiral followed by viscous smoothing across the turns of the spiral. The last computed state in Fig. 7 is composed of patches connected by thin sheets and a distorted region of vorticity. The total number of node points increased from 400 to 806 during the calculation. Up to the third frame, the circulation and impulse decreased by 0.1% but subsequently more inaccuracy resulted from the closeness of non-adjacent nodes. The integrand behaves logarithmically and polynomial quadrature is no longer accurate. Accurate computation of the integrals requires that the distance between quadrature points be smaller than the distance between non-adjacent nodes. At the last frame, these invariants have decreased by 1%. To continue this calculation further would require contour surgery which has been developed by Dritschel [9].

The final illustration is the head-on collision of two Norbury [22] rings with thickness parameter $\alpha = 1.0$. Fig. 8 shows successive instants during this collision. After the core has flattened at frame (d) it begins to "fillout" as in (e). At (h) a head of smaller aspect ratio has been formed. It is connected to a long flattened tail by a thin umbilical. Fig. 9 is a magnified view of the head and umbilical. It is remarkable that the shape of the head is fit well the two-dimensional Sadovskii–Pierrehumbert [30,24,25] vortex pair (dotted line) which propagates without change of form. This behavior is reminiscent of inelastic solitons [16].
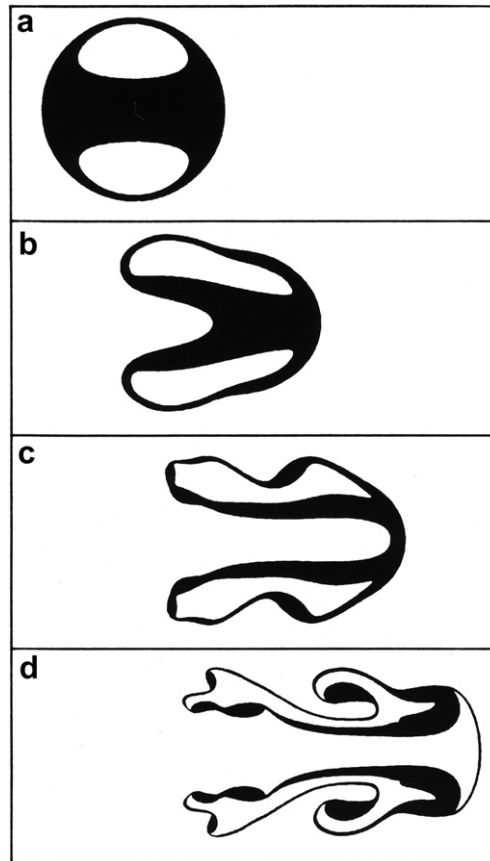
Fig. 7. Evolution of a vortex formed by removing a region of vortical fluid from Hill's spherical vortex. Times normalized using the mean toroidal radius and the speed of translation of the vortex without the hole: A, 0; B, 4.27; C, 8.53; D, 12.80.

The location of the vorticity centroid (plus sign) shows that roughly half the circulation resides in the tail. Owing to the considerable straining of the vortex boundaries near the collision plane and on the umbilical the total number of node points increased from 600 to 1972. Loss of accuracy began a few time steps prior to the last instant shown. This manifested itself as sharply increasing errors in the invariants. Nevertheless, the total change in the volume of vortical fluid was only .034%.

Fig. 10 shows that the head-tail structure has also been observed in experiments of two colliding rings obtained by [23]. The upper row (U) shows, at successive instants, the meridional plane illuminated by a sheet of light. The lower row (L) is an oblique view 30° to the plane of collision. In U(b) a head with a long tail similar to the contour dynamics result of Fig. 8h is seen. In the oblique view L(b) this appears as a concentration of smoke around the periphery of the flattened rings. In L(c) the head has pinched-off and moves independently of the tail. Probably due to slight asymmetry in the initial conditions U(c) shows that it moves at an angle from the collision plane. The tail also fails to remain planar. Nevertheless, axisymmetry is not broken until L(d) where the head develops the Crow [6] instability. Concentration of dye is seen at the periphery of the tail which may indicate the formation of another head. The head-tail structure has also been observed in three-dimensional vortex tube reconnection [31,19].

6. Summary

This work considered inviscid swirl-free axisymmetric flows consisting of regions in which the vorticity varies linearly with radius. The velocity field was expressed as a contour integral which reduces the problem to a one-dimensional integro-differential equation for the motion of the boundaries of the regions. The streamfunc-
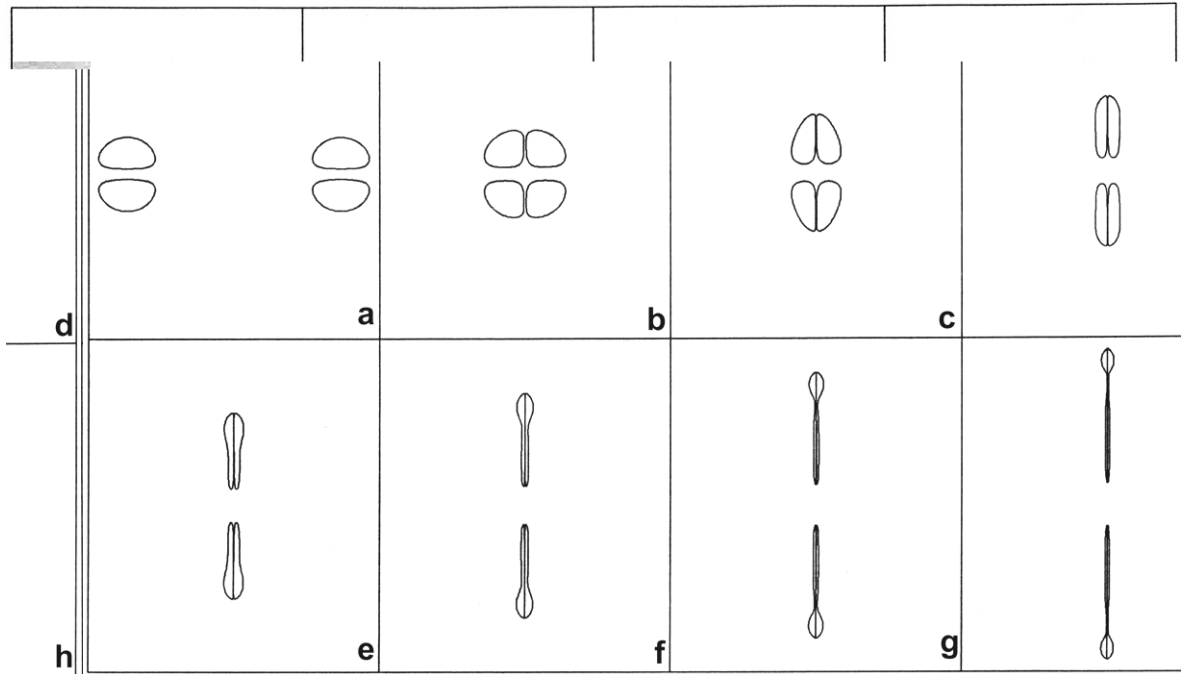
Fig. 8. Core shapes for the collision of $\alpha = 1.0, \hat{d} = 10$. +, vorticity centroids. U_0t/L_0: (a) 0; (b) 4.44; (c) 5.18; (d) 5.92; (e) 5.67; (f) 7.41; (g) 8.15; and (h) 8.89.
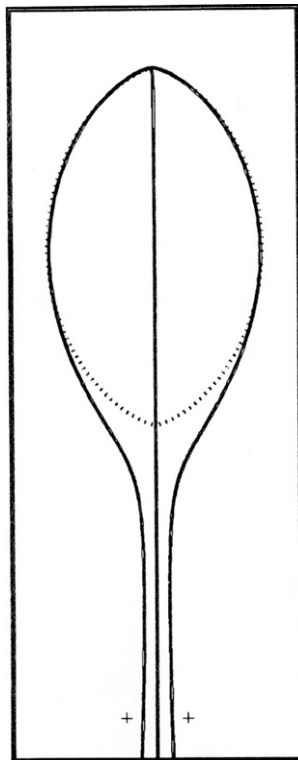

Fig. 9. Close-up of the head at $U_0t/L_0 = 8.89$ compared with the two-dimensional steadily translating vortex pair solution (. . ... .) of Sadovskii [30] and Pierrehumbert [24]. +, vorticity centroid.
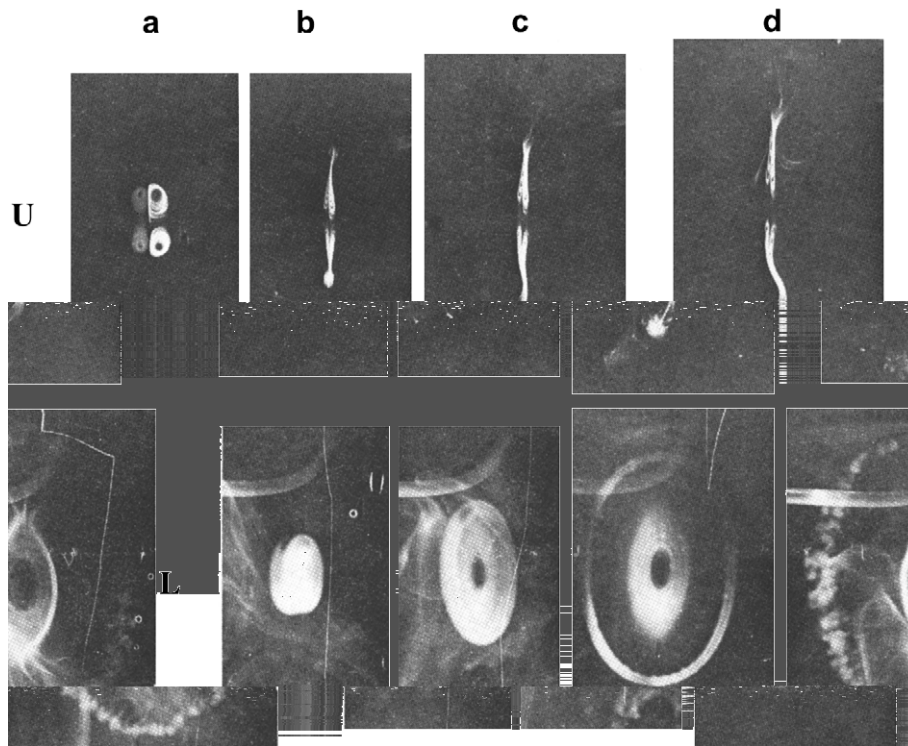
Fig. 10. Smoke visualization of the collision of two vortex rings by Oshima [23]. Time progresses from left to right. U: the upper series shows a meridional plane illuminated by a sheet of light; L: the lower series is an oblique view at 30° from plane of collision. Reproduced with permission.

tion was also formulated as a contour integral. The method was demonstrated for two vortex rings colliding head-on. A head-tail structure was formed which agrees with experimental flow visualization.

Tribute to Tony Leonard for this Special Issue Dedicated to Him

I was lucky when in 1983 Joel Ferziger hooked me up with Tony to do my dissertation. Tony was then a research scientist at NASA Ames. A few thoughtful words spoken by him often turned out to provide the key way of looking at something. And, he had a knack for making one feel I one knew the answer all along: in discussions he might preface his insight with I think you are trying to say this . . . '' I am certain that others can recount similar phenomena. Tony has a warm, easy-going, and supportive nature which endears him to all that meet him. That this co-exists with penetrating keenness makes him an ideal thesis adviser. His scientific motivations remain pure and untainted: the pursuit of truth, understanding, problem solving, and fun. Through a combination of acceptance, openness, and insight, Tony brings out the hidden and unrecognized value in whatever person or subject he touches. (KS).

Appendix A. Contribution to the induced velocity from adjacent segments

The purpose of this appendix is to obtain the contribution to the velocity at a given node point from segments which are adjacent to it. We proceed by expanding the kernel $\mathbf{K}(s')$ in (29) in a series of powers and logarithms. The series is then integrated exactly term by term.

Let the field point be the nth node located at (x_n, σ_n). Let (l_x, l_σ) be the axial and radial components of the vector with length l, pointing in the direction of integration along the forward adjacent segment. Then along this segment we have

$$x' = x_n + \xi l_x, \quad \sigma' = \sigma_n + \xi l_\sigma, \tag{40}$$

where ξ is a parameter which runs from 0 to 1 on the segment. The quantities A and B defined in (8) and (9), are along the segment

$$A = f\xi^2 + p\xi + q, \quad B = p\xi + q, \tag{41}$$

where

$$f = l^2, \quad p = 2\sigma_n l_\sigma, \quad q = 2\sigma_n^2. \tag{42}$$

The coefficients f, p and q above are functions of the segment geometry and the expansions of the kernels depend only on them. The contribution to the velocity at the nth node due to the segment is

$$\Delta u_\sigma = \mathcal{A} l_\sigma \int_0^1 \sigma' H \mathrm{d}\xi, \tag{43}$$

$$\Delta u_x = \mathcal{A} \left[-l_\sigma \int_0^1 (x_n - x') G \mathrm{d}\xi + l_x \int_0^1 \sigma_n H \mathrm{d}\xi \right]. \tag{44}$$

We provide expansions for each of the integrands which appears above. They are obtained with the aid of the expansions of the elliptic functions $K(\tilde{r})$ and $E(\tilde{r})$ about $\tilde{r} = 1$ given in Byrd and Friedman [3]. We write these out up to

$$\mathcal{O} \left[\log \left(\frac{4}{r^*} \right) r^{*4} \right], \tag{45}$$

where r^* is the complementary modulus $\sqrt{1 - \tilde{r}^2}$. The leading term in the expansion of r^* is $\mathcal{O}(\xi)$ so for consistency the highest power in ξ that may be retained in any term is four.

What does an expansion in r^* mean for our case? Let Δ denote the distance between the source and field points (in the same meridional plane), i.e.,

$$\Delta^2 = (x - x')^2 + (\sigma - \sigma')^2. \tag{46}$$

Define the parameter

$$\epsilon \equiv \frac{\Delta^2}{4\sigma\sigma'}. \tag{47}$$

Thus if the distance between source and field points is smaller than both their radii (σ and σ') then ϵ is small. Simply put, ϵ is small when local two-dimensionality holds for the line connecting the source and field points. Now

$$A + B = (x - x')^2 + \sigma^2 + \sigma'^2 + 2\sigma\sigma' = (x - x')^2 + \sigma^2 + \sigma'^2 - 2\sigma\sigma' + 4\sigma\sigma' = \Delta^2 + 4\sigma\sigma'$$
$$= 4\sigma\sigma'(1 + \epsilon), \tag{48}$$

while $B = 2\sigma\sigma'$ so that

$$r^{*2} = 1 - \frac{2B}{A + B} = \frac{\epsilon}{1 + \epsilon}. \tag{49}$$

Thus r^* is small when ϵ is small and our expansion will hold as long as local two-dimensionality prevails along the segment. This requires that the length of each segment be much smaller than the distance to the axis of its end-point closest to the axis. The body of the paper discussed how this condition is maintained.

Each of the integrands in (43) and (44) assumes the following form

$$\mathcal{C} \left[\log \left(\frac{8\sigma_n}{l\xi} \right) \sum_{j=0}^J c_j \xi^j + \sum_{j=0}^J c_j' \xi^j \right]. \tag{50}$$

For $\sigma' H$ and $\sigma_n H$, $J = 4$ but for $(x - x') G$ it is consistent to go up to $J = 5$ since $(x - x')$ is proportional to ξ. Each of the coefficients in (50) has the structure

$$c_j = a_j l_\sigma + b_j \sigma_n, \tag{51}$$

$$c'_j = a'_j l_\sigma + b'_j \sigma_n. \tag{52}$$

The following quantities recur often so it is convenient to define them at the outset.

$$T_1 = fpq^2, \quad T_2 = p^3 q, \quad T_3 = f^2 q^2, \tag{53}$$

$$T_4 = fp^2 q, \quad T_5 = p^4, \quad T_6 = fq^3, \tag{54}$$

$$T_7 = p^2 q^2, \quad T_8 = pq^3, \quad T_9 = q^4. \tag{55}$$

For $\sigma' H, J = 4$ and

$$
\begin{array}{ll}
a_4 = 288T_1 - 96T_2, & b_4 = 90T_3 - 216T_4 + 60T_5, \\
a'_4 = -384T_1 + 224T_2, & b'_4 = -93T_3 + 360T_4 - 152T_5, \\
a_3 = -576T_6 + 192T_7, & b_3 = a_4, \\
a'_3 = 192T_6 - 384T_7, & b'_3 = a'_4, \\
a_2 = -768T_8, & b_2 = a_3, \\
a'_2 = -a_2, & b'_2 = a'_3, \\
a_1 = -1536T_9, & b_1 = a_2, \\
a'_1 = 3072T_9, & b'_1 = a'_2, \\
a_0 = 0, & b_0 = a_1, \\
a'_0 = 0, & b'_0 = a'_1, \\
\mathcal{C} = -(1/2\pi)(1/1536q^4). &
\end{array} \tag{56}
$$

After the entries for $\sigma' H$ have been generated and stored, to obtain the corresponding entries for $\sigma_n H$ do the following. The b_j and b'_j for $\sigma_n H$ are the same as those for $\sigma' H$ which you have already stored. The a_j and a'_j for $\sigma_n H$ are zero; in other words you need worry only about the second terms in (51) and (52).

For $(x_n - x')G$, $J = 5$ and

$$
\begin{array}{ll}
a_5 = 288T_1 - 480T_2 & b_5 = 54T_3 - 360T_4 + 420T_5 \\
a'_5 = -384T_1 + 736T_2 & b'_5 = -63T_3 + 552T_4 - 704T_5 \\
a_4 = -192T_6 + 576T_7 & b_4 = a_5 \\
a'_4 = 192T_6 - 768T_7 & b'_4 = a'_5 \\
a_3 = -768T_8 & b_3 = a_4 \\
a'_3 = -a_3 & b'_3 = a'_4 \\
a_2 = 1536T_9 & b_2 = a_3 \\
a'_2 = 0 & b'_2 = a'_3 \\
a_1 = 0 & b_1 = a_2 \\
a'_1 = 0 & b'_1 = 0 \\
a_0 = 0 & b_0 = 0 \\
a'_0 = 0 & b'_0 = 0 \\
\mathcal{C} = -(1/2\pi)(t_x \sigma_n / 768q^5) &
\end{array} \tag{57}
$$

Finally, each integral is obtained by integrating (50) for $0 \leqslant \xi \leqslant 1$:

$$\mathcal{C}\left\{ \log\left(\frac{8\sigma_n}{l}\right) \sum_{j=0}^{J} \frac{c_j}{j+1} + \left[\sum_{j=0}^{J} \frac{c_j}{(j+1)^2} + \frac{c'_j}{j+1} \right] \right\}. \tag{58}$$

For the segment behind the node, if $(\tilde{l}_x, \tilde{l}_\sigma)$ are its components (in the direction of integration) then the expansions are identical except that $(-\tilde{l}_x, -\tilde{l}_\sigma)$ replace (l_x, l_σ) in forming f, p and q.

Appendix B. Contour formulation for the streamfunction

In the body of the paper, an expression for the velocity field was derived in terms of contour integrals. We now do the same for the Stokes streamfunction, ψ.

In calculating the shapes of steadily translating vortex rings, the condition that the streamfunction be constant on the surface of the vortex (in a steadily translating frame whose velocity is determined as part of the solution) is easier and more accurate to impose than one requiring that the velocity be tangent to the surface. Using the formulation one could compute the Prandtl–Batchelor eddy behind an axisymmetric body or calculate steady shapes more complicated than the Norbury [22] family, for example rings with nested contours. In his work, Norbury did not have available a contour formulation for the streamfunction and this necessitated costly and less accurate plane quadratures for the solution of the integral equation for steadily translating rings.

The vector potential, $\mathbf{A}$ is defined as

$$\mathbf{u} = \nabla \times \mathbf{A}, \tag{59}$$

$$\nabla \cdot \mathbf{A} = 0. \tag{60}$$

Given a certain $\mathbf{u}$, $\mathbf{A}$ is defined up to the gradient of a scalar function. The condition (60) is a convenient choice that makes $\mathbf{A}$ unique. Writing (59) in cylindrical coordinates and comparing it with the definition of the Stokes streamfunction one finds

$$\psi = \sigma A_\phi. \tag{61}$$

Hence, it is enough to calculate the vector potential. Eqs. (59) and (60) together imply

$$\nabla^2 \mathbf{A} = -\boldsymbol{\omega}, \tag{62}$$

whose solution for an unbounded fluid is

$$\mathbf{A} = \frac{1}{4\pi} \int_{\mathcal{D}} \frac{\boldsymbol{\omega}(\mathbf{x}')}{r} \mathrm{d}\mathbf{x}', \tag{63}$$

where $\mathcal{D}$ is the vorticity containing region. The goal is to transform this equation into a form in which the integrand is concentrated on the boundary. First, as noted previously $1/r = \nabla'^2 r/2$, so that

$$\mathbf{A} = \frac{1}{8\pi} \int_{\mathcal{D}+} \boldsymbol{\omega}(\mathbf{x}')\nabla'^2 r \mathrm{d}\mathbf{x}'. \tag{64}$$

Note that we have changed the domain of integration from $\mathcal{D}$ to $\mathcal{D}+$ which is defined to be slightly larger than $\mathcal{D}$. This is permissible since the vorticity is zero in the extra region. The reason for this change will become clear below. Next, we write Green's second identity for the pair of functions $\boldsymbol{\omega}$ and r:

$$\int_{\mathcal{D}+} (\boldsymbol{\omega}\nabla'^2 r - r\nabla'^2 \boldsymbol{\omega})\mathrm{d}\mathbf{x}' = \int_{\partial\mathcal{D}+} \left(\boldsymbol{\omega}\frac{\partial r}{\partial n'} - r\frac{\partial \boldsymbol{\omega}}{\partial n'}\right)\mathrm{d}S. \tag{65}$$

The reason for using the slightly larger region $\mathcal{D}+$ now becomes clear. Since $\partial\mathcal{D}+$ lies in a region of identically zero vorticity, the boundary integral in (65) vanishes giving:

$$\int_{\mathcal{D}+} \boldsymbol{\omega}(\mathbf{x}')\nabla'^2 r \mathrm{d}\mathbf{x}' = \int_{\mathcal{D}+} r\nabla'^2 \boldsymbol{\omega}(\mathbf{x}')\mathrm{d}\mathbf{x}'. \tag{66}$$

The introduction of $\mathcal{D}+$ was suggested to us by P. Spalart. Decompose the right hand side of (66) into two parts, one for the interior of $\mathcal{D}+$ and another for a thin shell of width 2ε which surrounds $\partial\mathcal{D}$. Then take the limit as $\varepsilon \to 0$. The first part vanishes because the Laplacian of the linear vorticity is zero. As an aside, one might think at this point that the formulation could be used to obtain steady vortex rings with vanishing $\nabla^2 \boldsymbol{\omega}(\mathbf{x})$ in $\mathcal{D}$ which includes but is more general than the linear in radius vorticity distribution. Such steady flows are called "controllable" by the Truesdell school of mechanics. Unfortunately, however, Marris and Aswani [18] have provided a long and complicated proof that the only non-rectilinear controllable axisymmetric motions are those in which $\omega_\phi/\sigma = \text{constant}$.

To work out the integral in the shell, introduce orthogonal curvilinear coordinates (n, s, ϕ) such that the surfaces $n = -\varepsilon, 0, \varepsilon$ coincide with the inner boundary of the shell, the surface of the vortex and the outer boundary of the shell, respectively. If s and n are chosen to be the arc lengths on the lines along which they vary then the metrics are $(h_n, h_s, h_\phi) = (1, 1, \sigma)$. With these metrics the Laplacian becomes

$$\nabla^2 \boldsymbol{\omega}(\mathbf{x}) = \nabla^2 [\omega_\phi(s, n) \hat{\boldsymbol{\phi}}] = \frac{\partial}{\partial n} \left[\frac{1}{\sigma} \frac{\partial(\sigma \omega_\phi)}{\partial n} \right] \hat{\boldsymbol{\phi}} + \mathcal{O}(\varepsilon), \tag{67}$$

$$\hat{\boldsymbol{\phi}} = -\sin\phi \hat{\mathbf{y}} + \cos\phi \hat{\mathbf{z}}, \tag{68}$$

where $\mathcal{O}(\varepsilon)$ denotes terms which disappear upon integration as $\varepsilon \to 0$. These arise from tangential (s) derivatives of the vorticity. As before, let us choose the field point to be on the $\phi = 0$ plane where $A_\phi = A_z$ and $r = \sqrt{A - B\cos\phi'}$ with A and B as defined in (8) and (9). Then

$$A_\phi(x, \sigma) = \frac{1}{8\pi} \lim_{\varepsilon \to 0} \int_0^{2\pi} \mathrm{d}\phi' \cos\phi' \oint \mathrm{d}s' \int_{-\varepsilon}^{+\varepsilon} \mathrm{d}n' \sigma' r \frac{\partial}{\partial n'} \left[\frac{1}{\sigma'} \frac{\partial(\sigma' \omega_\phi)}{\partial n'} \right]. \tag{69}$$

Denote the innermost integral in (69) by I_n. Applying integration by parts twice gives

$$I_n = \sigma' r \left[\frac{\partial \omega_\phi}{\partial n'} \right]_{-\varepsilon}^{+\varepsilon} - \sigma' \frac{\partial r}{\partial n'} \left[\omega_\phi \right]_{-\varepsilon}^{+\varepsilon} + \mathcal{O}(\varepsilon). \tag{70}$$

In the limit as $\varepsilon \to 0$

$$\left[\omega_\phi \right]_{-\varepsilon}^{+\varepsilon} \to -\mathcal{A}\sigma', \tag{71}$$

$$\left[\frac{\partial \omega_\phi}{\partial n'} \right]_{-\varepsilon}^{+\varepsilon} \to -\mathcal{A}\sin\theta'. \tag{72}$$

Finally,

$$\psi(x, \sigma) = \frac{\mathcal{A}\sigma}{8\pi} \oint \mathrm{d}s' \left(\sigma'^2 \int_0^{2\pi} \frac{\partial r}{\partial n'} \cos\phi' \mathrm{d}\phi' - \sigma' \sin\theta' \int_0^{2\pi} r \cos\phi' \mathrm{d}\phi' \right). \tag{73}$$

The two integrals with respect to ϕ' can be expressed explicitly in terms of tabulated integrals denoted as I_1, I_2 and I_3 below. The first is obtained after substituting for $\partial r / \partial n'$ from (26) and (28) and the second after an integration by parts:

$$\int_0^{2\pi} \frac{\partial r}{\partial n'} \cos\phi' \mathrm{d}\phi' = 2[(x' - x)I_2 \cos\theta' - \sigma I_3 \sin\theta' + \sigma' I_2 \sin\theta'], \tag{74}$$

$$\int_0^{2\pi} r \cos\phi' \mathrm{d}\phi' = B(I_3 - I_1), \tag{75}$$

where

$$I_1 \equiv \int_0^\pi \frac{\mathrm{d}\phi'}{\sqrt{A - B\cos\phi'}} = \frac{2}{\sqrt{A + B}} K(\tilde{r}), \tag{76}$$

$$I_2 \equiv \int_0^\pi \frac{\cos\phi'}{\sqrt{A - B\cos\phi'}} \mathrm{d}\phi' = \frac{2A}{B\sqrt{A + B}} K(\tilde{r}) - \frac{2}{B}\sqrt{A + B} E(\tilde{r}), \tag{77}$$

$$I_3 \equiv \int_0^\pi \frac{\cos^2\phi'}{\sqrt{A - B\cos\phi'}} \mathrm{d}\phi' = \frac{2}{3B^2\sqrt{A + B}} [(2A^2 + B^2)K(\tilde{r}) - 2A(A + B)E(\tilde{r})], \tag{78}$$

$$\tilde{r} = \sqrt{\frac{2B}{A + B}}. \tag{79}$$

This formulation was checked numerically against the exact expression for Hill's spherical vortex given in Batchelor [1, eq. 7.2.18] relative to a reference frame travelling with the vortex. For example, at the point where the streamfunction has a peak, the errors with 15, 30 and 60 segments were -2.4%, $-.61\%$ and $-.15\%$, respectively, indicating the second order convergence of the segment discretization.

References

[1] G.K. Batchelor, An Introduction to Fluid Dynamics, Cambridge University Press, Cambridge, UK, 1973.

[2] D. Bierens de Haan, Nouvelles Tables d'Integrales Définies, G.E. Stechert and Co., New York, 1939.

[3] P.F. Byrd, M.D. Friedman, Handbook of Elliptic Integrals for Scientists and Engineers, Springer Verlag, New York, 1971.

[4] W.J. Cody, Chebychev approximations for the complete elliptic integrals K and E, Math. Comput. 19 (1965) 105–112.

[5] J.A. Crow, Quadrature of integrands with a logarithmic singularity, Math. Comput. 60 (201) (1993) 297–301.

[6] S.C. Crow, Stability theory for a pair of trailing vortices, AIAA J. 8 (1970) 2172–2179.

[7] D.G. Dritschel, The stability and energetics of corotating uniform vortices, J. Fluid Mech. 157 (1985) 95–134.

[8] D.G. Dritschel, The non-linear evolution of rotating configurations of uniform vorticity, J. Fluid Mech. 172 (1986) 157–182.

[9] D.G. Dritschel, Contour surgery: A topological reconnection scheme for extended integrations using contour dynamics, J. Comp. Phys. 77 (1988) 240–266.

[10] D.G. Dritschel, Vortex properties of two-dimensional turbulence, Phys. Fluid A 5 (1993) 984–997.

[11] F.W. Dyson, The potential of an anchor ring – part II, Phil. Trans. Roy. Soc. Lond. A 184 (1893) 1041–1106.

[12] P.-A. Gourdain, J.-N. Leboeuf, Contour dynamics method for solving the Grad–Shafranov equation with applications to high beta equilibria, Phys. Plasmas 11 (2004) 4372–4381.

[13] I.S. Gradshteyn, I.M. Ryzhik, Table of Integrals, Series, and Products, Academic Press, New York, 1980.

[14] H. Helmholtz, On integrals of the hydrodynamical equations which express vortex-motion, Phil. Mag. J. Sci. (Fourth Series) 33 (1867) 485–512, This reference is a translation by P.G. Tait of Helmholtz's original 1858 paper.

[15] M.A. Jawson, G.T. Symm, Integral Equation Methods in Potential Theory and Elastostatics, Academic Press, New York, 1973.

[16] J.C. Lewis, J.A. Tjon, Resonant production of solitons in the rlw equation, Phys. Lett. A 73 (1979) 275–279.

[17] S.J. Lin, G.M. Corcos, The mixing layer: deterministic models of a turbulent flow. Part 3 the effect of plane strain on the dynamics of streamwise vortices, J. Fluid Mech. 141 (1984) 139–178.

[18] A.W. Marris, M.G. Aswani, On the general impossibility of controllable axisymmetric Navier–Stokes motions, Arch. Ration. Mech. Anal. 63 (1977) 107–153.

[19] M. V Melander, F. Hussain, Cross-linking of two antiparallel vortex tubes, Phys. Fluids A 1 (4) (1989) 633–636.

[20] H.K. Moffatt, D.W. Moore, The response of Hill's spherical vortex to a small axisymmetric disturbance, J. Fluid Mech. 78 (1978) 749–760.

[21] J.C. Neu, The dynamics of a columnar vortex in an imposed strain, Phys. Fluids 27 (10) (1984) 2397–2402.

[22] J. Norbury, A family of steady vortex rings, J. Fluid Mech. 57 (1973) 417–431.

[23] Y. Oshima, Head-on collision of two vortex rings, J. Phys. Soc. Japan 44 (1978) 328–331.

[24] R.T. Pierrehumbert, A family of steady, translating vortex pairs with distributed vorticity, J. Fluid Mech. 99 (1980) 129–144.

[25] R.T. Pierrehumbert, Corrigendum, a family of steady, translating vortex pairs with distributed vorticity, J. Fluid Mech. 102 (1981) 478.

[26] W. Poppe, Theoretische Untersuchung stationärer Ringwirbelströmungen mit unstetiger Wirbelstärkenverteilung. Technical Report 29/1978, Max-Planck-Institut Für Strömungsforschung, Göttingen, 1978.

[27] C. Pozrikidis, The non-linear stability of Hill's vortex, J. Fluid Mech. 168 (1986) 337–367.

[28] D.I. Pullin, Contour dynamics methods, Ann. Rev. Fluid Mech 24 (1992) 89–115.

[29] D.I. Pullin, P.A. Jacobs, Inviscid evolution of stretched vortex arrays, J. Fluid Mech. 171 (1986) 377–406.

[30] V.S. Sadovskii, Vortex regions in a potential stream with a jump of bernoulli's constant at the boundary, Appl. Math. Mech. 35 (1971) 729–735.

[31] P.R. Schatzle, An experimental study of fusion of vortex rings. Ph.D thesis, California Institute of Technology, 1987.

[32] R.N.L. Smith, Direct gauss quadrature formulae for logarithmic singularities on isoparametric elements, Eng. Anal. Bound Elem. 24 (2000) 161–167.

[33] M. Sun, S. Lichter, Entrainment and detrainment from a model boundary layer, J. Fluid Mech. 485 (2003) 143–159.

[34] N.J. Zabusky, M.H. Hughes, K.V. Roberts, Contour dynamics for the Euler equations in two-dimensions, J. Comp. Phys. 30 (1979) 96–106.